Physical-Chemical Methods of Modeling in Nonlinear and Relaxed Optics

Petro P. Trokhimchuck*

Anatoliy Svidzinskiy Department of Theoretical and Computer Physics, Lesya Ukrayinka Volyn' National University, 13 Voly Avenue, 43025, Lutsk, Ukraine

***Corresponding Author:** Petro P. Trokhimchuck, Anatoliy Svidzinskiy Department of Theoretical and Computer Physics, Lesya Ukrayinka Volyn' National University, 13 Voly Avenue, 43025, Lutsk, Ukraine*

Abstract: *Main physical–chemical methods of modelling the Nonlinear and Relaxed Optical processes and phenomena is analyzing. The difference between Nonlinear Optical and Relaxed Optical processes is shown. The former are non-equilibrium, while the latter are irreversible in nature. G. Haken put the idea of an analogy between phase transitions and nonlinear optical phenomena forward. He used L. Landau's thermodynamic theory of phase transitions for this purpose. From a physical-chemical point of view, nonlinear optical phenomena and processes are caused by the absorption of light at impurity centers, the concentration of which is usually 5-7 orders of magnitude lower than the concentration of atoms of the base material. Relaxed-optical processes are associated with more intense light absorption, including the region of the material's self-absorption. In this case, depending on the intensity of irradiation, we have a whole cascade of phenomena and processes (from optical pumping of laser radiation to the corresponding phase transformations of the irradiated material). To model such processes, we must use crystallographic lattices or phase diagrams of the irradiated material. For modeling such processes as laser-induced optical breakdown of a transparent material, we must also use physical-chemical modeling methods to establish the self-focusing mode and the actual optical breakdown at the maximum of the interferograms formed by the short-wavelength part of the secondary Cherenkov radiation. For the case of focused radiation irradiation, the first part of the modeling is not needed. In general, physical-chemical modeling methods more fully reflect the specifics of the interaction of laser radiation with matter at the microscopic level, including both the phenomena and processes of Nonlinear and Relaxed Optics.*

Keywords: *physical–chemical methods, Nonlinear Optics, Relaxed Optics, critical processes, phase transformations, nonequilibrium phenomena, irreversible processes.*

1. INTRODUCTION

Main physical–chemical methods of modelling the Nonlinear and Relaxed Optical processes and phenomena is analyzing [1 – 23]. The main difference lies in the nature of the phenomena and processes. Nonlinear optical processes have a non-equilibrium nature [2 – 6], while relaxed optical processes are usually irreversible [1, 6 – 13, 23]. This difference is due to the specifics of these sciences. Nonlinear optics (NLO) is the branch of optics that describes the behavior of light in nonlinear media, that is, media in which the polarization density P responds non-linearly to the electric field E of the light [6]. The non-linearity is typically observed only at very high light intensities (when the electric field of the light is $>10^8$ V/m and thus comparable to the atomic electric field of $\sim 10^{11}$ *V/m*) such as those provided by lasers. Above the Schwinger limit, the vacuum itself is expected to become nonlinear. In nonlinear optics, the superposition principle no longer holds. Relaxed Optics (RO) studies in a broader sense the processes of secondary relaxation of primary optical excitations in a medium [1, 7 – 13]. In this case, it includes Linear and Nonlinear Optics, which are "responsible" for radiative relaxation. The same part, which is responsible for non-radiative relaxation, is Relaxed Optics in the narrower sense of the word [1]. It is understood that both non-equilibrium and irreversible processes and phenomena are caused by short-lived or long-lived physical-chemical changes in the environment [1]. Knowledge of the mechanisms of these changes allows us to explain the microscopic nature of the corresponding phenomenon or process.

Let's first analyze how this is modeled in Nonlinear Optics. First concept was represented by H. Haken [2]. He put the idea of an analogy between phase transitions and nonlinear optical phenomena forward. He used L. Landau's thermodynamic theory of phase transitions for this purpose. He analyzed the possibility of describing nonlinear optical phenomena by phase transitions of the first and second order.

These studies were later developed in [3, 4]. In this case, we can formally attribute one or another phase transition to certain nonlinear optical phenomena and processes, but it is quite difficult to talk about any microscopic mechanisms of the phenomenon.

Formal analogy between second order phase transitions and synergetic was made and analyzed , including by H. Haken [2].

This analogy can be legitimizing with help de Broglie formula (1). This formula is represented the equivalence between ordered and disordered information for closed system [7, 24].

$$\frac{S_a}{\hbar} = \frac{S_e}{k_B}, \tag{1}$$

where S_a – action, S_e – entropy, $\hbar$ – reduced Planck's constant, k_B – Boltzman constant.

This approach was also applying to first order phase transitions [2].

From a physical-chemical point of view, nonlinear optical phenomena and processes are caused by the absorption of light at impurity centers, the concentration of which is usually 5-7 orders of magnitude lower than the concentration of atoms of the base material [2]. That is why the main methods for modeling classical nonlinear optics are classical and quantum electrodynamics (perturbation theory can be used, and all nonlinear optical phenomena are nothing more than perturbations caused by the nonlinear polarization of the medium) [6]. Physical-chemical processes are implicitly included in the nonlinear polarization of the medium [8]. From a temporal point of view, nonlinear optical phenomena are forming in times that are approximately equal to the generation time of the nonlinear polarization and its lifetime. This approach does not allow for adequate description of such processes as time delay of certain nonlinear optical phenomena, aging of laser and nonlinear optical media, processes of laser radiation chaos, laser-induced breakdown of media, etc [1]. In addition, it is necessary to somehow describe nonlinear processes associated with the medium's self-absorption; this area is poorly studied in classical Nonlinear Optics [1, 2, 5, 6].

Relaxed Optics was created in order, on the one hand, to supplement the explanation of Nonlinear Optics processes that could not be adequately explained using the theoretical apparatus of nonlinear optics, and on the other hand, it was necessary to create the physics of laser technologies [7 – 13].

From this point of view, Relaxed Optics can be considered as an extension of Nonlinear Optics to the phenomena and processes of non-radiative relaxation [1].

That is why Relaxed Optics is a synthesis of such sciences as: solid-state radiation physics, physical chemistry, nonlinear optics, quantum electronics, physics of critical phenomena, etc [1].

Thus, one of the basic concepts of solid-state radiation physics is the Seitz energy – the energy required to break all the closest chemical bonds of an atom in a crystal [8, 9]. The energies of incident particles in solid-state radiation physics (ions, electrons, neutrons, gamma quanta) are much greater than the energies of optical photons [8]. Therefore, the processes of irreversible interaction of laser radiation with matter are too soft for solid-state radiation physics and too hard for Nonlinear Optics. In this case, we have to move from atoms and electronic states to the types of individual chemical bonds and, in addition, take into account the excitation saturation regime (laser effect). It is the excitation saturation regime that allows us to move from the long-range to the short-range approximation regime. At the same time, we can base such concepts on broken bonds, polyphase transformations, cascade processes, etc [8, 9].

Based on this, three main concepts of RO were created.

The first concept is kinetic-dynamic [1], it is based on the phenomenological classification of phenomena of the processes of interaction of optical radiation with matter, based on their energy, time, geometric and concentration characteristics. On its basis, all phenomena of the interaction of optical radiation with matter were explained, including linear and non-linear optics. The phenomena and processes of Relaxed Optics themselves were also classified.

The second concept is electromagnetic [1]. It is an extension of the concept of nonlinear optics: the expansion in a series of powers of the electric field strength of the polarization of the medium, into irreversible phenomena. For this, the Poynting tensor was used as the product of electric and magnetic induction with their expansion in a series of powers of the electric and magnetic field strengths.

The third concept is coherent [1]. It was built on the basis of the concept of coherent structures, which is a generalization of the classical concepts of coherence and their transfer to structures. Its classifications echo the classifications of the kinetic-dynamic concept.

It should be noted that most relaxation-thermal processes have a cascade nature. Based on this, the concept of photochemical efficiency with the Stark-Einstein principle [5] was generalized to the concept of photonic efficiency with the generalized Stark-Einstein principle.[9]. In this case, differential photon efficiency was introduced for simple processes and integral photon efficiency for cascade processes. In addition, a coherence zone was introduced for cascade processes. This allows us to distinguish a short-range cascade from long-range purely dynamic processes (thermal and plasma).

It was also showing that, along with thermodynamic nucleation processes, electromagnetic nucleation processes are also effective in a number of cases [8]. In particular, these theories include the cascade model of excitation of chemical bonds in the excitation saturation regime [1, 7 – 9] and the electrostatic phase model of V. Stafeev [8], which is based on the idea of chemical affinity.

It should be noted that neglecting short-range processes in the excitation saturation regime and using long-range thermal and plasma models often lead to contradictory explanations of experimental data.

Relaxed-optical processes are associated with more intense light absorption, including the region of the material's self-absorption [1]. In this case, depending on the intensity of irradiation, we have a whole cascade of phenomena and processes (from optical pumping of laser radiation to the corresponding phase transformations of the irradiated material). To model such processes, we must use crystallographic lattices or phase diagrams of the irradiated material.

2. MAIN RESULTS

Let us now analyze the models used to explain the experimental results of laser radiation with antimonite and indium arsenide.

The profiles of the distribution the photostimulated donor centers in subsurface layers *InSb* and *InAs* are represented in Figure1 [1]. The samples of p-type conductivity are irradiated by pulses Ruby laser (pulse duration 20 *ns*, wavelength 0.6943 *μm*). For intensity of irradiation $I_0 > 0.01$ *J·cm*$^{-2}$ for *InSb* and $I_0 > 0.012$ *J·cm*$^{-2}$ for *InAs* the n-layers on *p*-type materials are created.

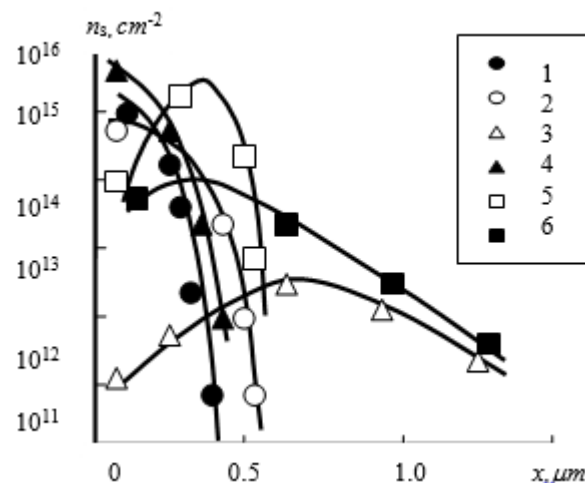**Figure 1.** *The profiles the distribution the layer concentration of the donor centers in inverse layers InSb and InAs after Ruby laser irradiation with various density of energy (monoimpulse regime): 0,07 (1); 0,1 (2); 0,16 (3); 0,16 (4); 0,25 (5); 0,5 J·cm^{-2} (6). 1-3—InSb, 4-6—InAs* [1].

For intensity of irradiation $I_0 < 0.1$ *J·cm*$^{-2}$ for *InSb* and $I_0 < 0.16$ J·cm^{-2} for *InAs* the profiles of the distribution of donor centers are represented the Buger-Lambert law (law of absorption the light in homogeneous media). For further increasing the irradiated intensity the profiles of the concentration donor centers have diffusion nature. The visible destruction of the irradiated semiconductor melting, the change of the surface color) had place for $I_0 > 0.3$ *J·cm*$^{-2}$ for *InSb* and $I_0 > 0.5$ *J·cm*$^{-2}$ for *InAs*. This effect has oriental character [1]. For crystallographic direction {111} the process of the creation damages is more effective as for direction {110}.

The profiles of a distribution of donor centers in *InSb* after laser irradiation are representing in Figure 2 [25]. An irradiation was created with help Ruby laser ($\lambda = 0.69\mu m, \tau_i = 5 - 6\ ms$) and series of pulses Nd:YAG laser ($\lambda = 1.06\mu m, \tau_i = 10\ ns$ frequency of repetition of impulses was 12.5 Hz). The dependence of layer concentration of electrons after Ruby laser irradiation is represented in Fig.2 [25]. A value of threshold the energy of creation n-layers is equaled $\sim 5^{J}/_{cm^2}$. A tendency of the saturation the layer concentration had place for the energy density $\sim 30\ ^{J}/_{cm^2}$. The melting of surface has place for this value of the irradiation.
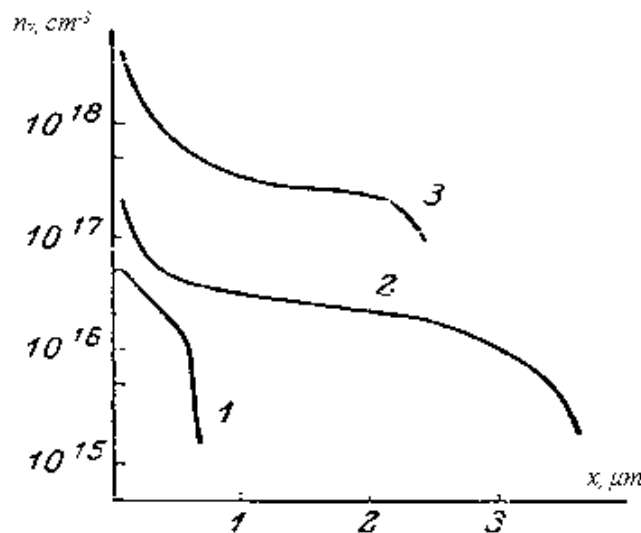

Figure2. *Profiles of the volume distribution electrons after laser irradiation. 1, 2 – Ruby laser; 3 – YAG:Nd laser. Energy density in pulse J/cm²:* $^{j}/_{c^2}$: 1 – 5; 2 – 40 [25].

The explanation of the shape of the distribution profiles shown in Fig. 1 was carried out using a modified photoelectric effect model. A system of diffusion and thermal conductivity equations was derived. Neglecting surface phenomena for layer concentrations, the following relations were obtained:

$$n_s = \frac{\alpha\eta(1-R)I_0\tau_i x}{h\nu(\alpha^2 L^2 - 1)\tau_r}\left[\alpha L\exp\left(-\frac{x}{L}\right) - \exp(-\alpha x)\right]. \tag{2}$$

where α is absorption index, η – index of generation of laser-induced donor centers, R – light reflectance, τ_i – irradiation time, τ_r – relaxation time, L – diffusion length, ν – frequency of irradiation light, I_0 – intensity of irradiation, x – the depth of corresponding layer [1].

The relaxation time τ_r is determined from functional dependence a temperature $T(x,t)$) for each layer and corresponding diffusion coefficient is determined as

$$D = D_0 exp\left(-\frac{E_a}{k_B T}\right). \tag{3}$$

Where E_a is activarion energy of diffusion [1].

From (2) we can receive two border approximations. First is named kinetic ($\alpha L \ll 1$)

$$n_{k_s} = \frac{\alpha\eta I_0 \tau' x}{h\nu\tau_r}\exp(-\alpha x) \tag{4}$$

and second is named dynamic   ($\alpha L \gg 1$)

$$n_{k_D} = \frac{\eta(1-R)I_0\tau' x}{h\nu L\tau_r}\exp\left(-\frac{x}{L}\right). \tag{5}$$

To explain the microscopic nature of the generation of laser-induced yule centers, a two-dimensional sphalerite lattice was used (this is the symmetry of the irradiated antimonide and indium arsenide crystals) on basis of Figure 3.

Bond 1 is corresponded to band gap and has value 0,18 eV, bond 2 – 1,95 eV and bond 3 – 2,15 eV [1]. For InAs bond 1 has value 0,36 eV, bond 2 – 3,8 eV and bond 3 – 4,2 eV [11, 13].
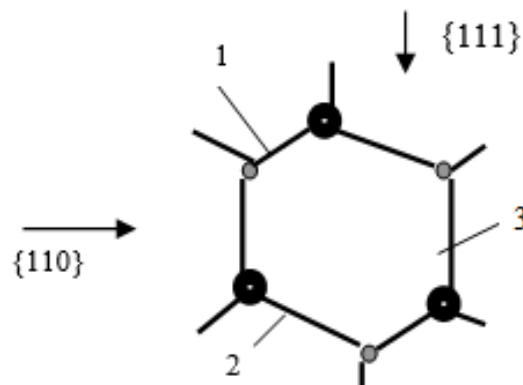
Figure3. *Two-dimensional picture the crystal lattice A_3B_5 (including InSb and InAs) the cubic symmetry.*

Bond 1 is pure covalent [1].

In this case, we have one mechanism of light scattering (absorption) in media. In further, we select D_0 = 0,05 cm^{-2}·s^{-1} is coefficient of the self-diffusion atoms of *In*; E_a=1,81 *eV* is energy of the activity the own diffusion atoms of *In* [1]; relaxation time τ_r is determined with functional dependence $T(t)$ and equal $(10 \div 10^3)\,\tau_i$; $\tau' \sim 10^{-7}s$ – the time of the life the unstable carriers in crystal [6]; R= 0,45 for $h\nu$ =1,78 *eV*; η = 0,2 (ionic mechanism); α =2·10^5 cm^{-1}; τ_1 =2·10^{-8} s. The binding calculated results to experimental data were provided for $I_0 = 0.1 {J}/{cm^2}$.

Method of the estimation of level of saturated excitation of proper chemical bonds may be used for the selection of optimal regime for optical pumping of semiconductor laser [1] and for creation stable $n-p$ -junctions on semiconductors [1] and for the creation layers with new phases, including nanostructures [1].

For these crystals the energy of these bonds are equaled the energy of band gap E$_g$ (0,18 *eV* for *InSb* and 0,36 *eV* for *InAs* at room temperature). On Fig. 3 this bond is signed as 1. For this bond ions *In* and *Sb* (or *In* and *As*) are placed on minimal distance (the sum of proper covalent radiuses). Other chemical bonds in this crystal symmetry have more long sizes. With geometrical point of view in crystal direction {111} the cross section of effective interaction the light quantum with bond 1 is more effective than for direction {110}. The angle among bond 1 and direction {110} is 37,5º. Quanta of ruby laser in linear regime of the irradiation are not interacted with another bonds practically because it energies are less than energy of this bond. The correlation of effective square of bond 1 for directions {110} and {111} is explained the oriental effect of creation donor centers [1].

For one coefficient of diffusion the general view of the formula for the profile of distribution of donor centers has form (2) [1].

Further we used kinetic (formula (4)) and dynamic (formula (5)) approximations. Diffusion length is determined by means of correlation:

$$L = \sqrt{D\tau_r}\,. \tag{6}$$

It should be noted that the profiles of distribution are necessary to be calculated using a formula (6). However at the calculation of the left part of the curves 2 and 3 of Figure2 (subsurface area) it is possible to use correlation (5), and at the calculation of right part of curves2 and 3 is correlation (5).

Go across now from the one-diffusive approximation [1] to two-diffusive and use these results for the modelling for *InSb* and *InAs*. Instead of diffusion of donor centers will examine self-diffusion of atoms of indium and antimony, which are caused by the secondary effects of relaxation optics. As known from literature [1] the atoms of indium and antimony or indium and arsenic have different coefficients of self-diffusion. The coefficient of self-diffusion (more correct it will be to say the photostimulated diffusion) of atoms of antimony less than of atoms of indium [1].

Literary data for self-diffusion of atoms of indium and furnace in the indium antimonite are contradictory [1]. Therefore will use those data that correspond to experimental data, namely, the coefficient of self-diffusion of atoms of indium is higher, than of antimony.

For the estimation of diffusive "tails" of curves 3 and 6 of Fig. 6, we are using modified formula (5) for the ions of antimony and indium or indium and arsenic [1] .

Concordantly [1] temperature dependence of coefficients of diffusion has next form

$$D_i = D_{0i} exp\left(-\frac{Q_i}{kT}\right), \ i \in (In, Sb), \tag{7}$$

where Q_i – proper activation energy of self-diffusion.

For a calculation the corresponding diffusion coefficients we select next data [1]

$$D_{0In} = 1.76 \cdot 10^{13} \ cm^2/s, , D_{0Sb} = 3.1 \cdot 10^{13} \ cm^2/s. \tag{8}$$

Procedure of further calculation was next. The descriptions resulted in got out for a calculation [1], however correlation of energies of activation of self-diffusion undertook to such as in [1, 7 – 13], what correspond to experimental data. Then in obedience to formula (7) the coefficient of self-diffusion of antimony was estimated for the temperature of 800K (temperature of melting of indium antimonide [1]). In future a scenario of calculation was following. Diffusive length of 0,7 μm (curve 3 Fig.1) is corresponded to diffusion of antimony, as we get the inverted layer of donor type on substrate of p-type. Relaxation time is equalled $\tau_r = 10^3 \tau_i = 2 \cdot 10^{-5} s$. As result, the coefficient of diffusion of atoms of antimony is determined from equation:

$$D_{Sb} = \frac{L_{Ab}^2}{\tau_r} = 2.45 \cdot 10^{-4} \ cm^2/s. \tag{9}$$

The obtained calculation data allow quality to explain behaviour of "tails" of curves of Figure 1. Depth of formation of donor centers for a curve 3 of Fig.1 (~1,5 μm) approximately corresponded a depth on that the concentration of centers of p-type (atoms of indium) becomes more than concentration of centers of n-type (atoms of antimony). From the value of this length, which is calculated according to correlation $x_{eq} = \frac{L_{In}L_{Sb}}{L_{In}-L_{Sb}} \ln \frac{L_{In}}{L_{Sb}} = 1.5 \ \mu m$, we get diffusive run-length of atoms of indium $L_{In} = 4.2\mu m$.

The coefficient of diffusion of atoms of indium is determined like analogous to antimony and equal

$$D_{In} = \frac{L_{In}^2}{\tau_r} = 8.82 \cdot 10^{-3} \ cm^2/s. \tag{10}$$

Having these data, we can now define activation energies of the photostimulated diffusion of indium and antimony atoms. They are determined from equation

$$Q_{In(Sb)} = kT \ln \frac{D_{0In(Sb)}}{D_{In(Sb)}}. \tag{11}$$

After substitution of corresponding data, we have $Q_{In} = 2.45 \ eV$, $Q_{Sb} = 2.71 \ eV$. Literary data [1] give value $Q_{In} = Q_{Sb} = 4.3 \ eV$. These data behave to material of n-type. We have an irradiation of material of p-type, and for this material the atoms of indium have greater mobility than atoms of antimony. Naturally, we must take into account and diffusion (radiation (photo) stimulated [1]) that decreases energy of activation.

Analogous results were receiving for indium arsenide [1]. Data for estimation was next $D_{0In} = 6 \cdot 10^5 \ cm^2/s$, $D_{0As} = 3 \cdot 10^7 \ cm^2/s$, relaxation time $\tau_r = 10^3 \tau_i = 2 \cdot 10^{-5} s$. Diffusion length of As atoms is equal 0,7 μm (for curver 6 of Fig.2). From the value of this length, which is calculated according to correlation $x_{eq} = \frac{L_{In}L_{As}}{L_{In}-L_{As}} \ln \frac{L_{In}}{As} = 1.5 \ \mu m$, we get diffusive run-length of atoms of indium $L_{In} = 4.2\mu m$. Proper coefficients of self-diffusion are equaled $D_{In} = \frac{L_{In}^2}{\tau_r} = 3 \cdot 10^2 \ cm^2/s$, $D_{As} = \frac{L_{As}^2}{\tau_r} = 8 \cdot 10^{-4} \ cm^2/s$ and energy of diffusion activation $- Q_{In} = 1.76 \ eV$, $Q_{As} = 2.8 \ eV$.

The represented two-diffusive model over shows as far as effective there can be an account of different mobility of atoms-components of semiconductor (in this case indium antimonite) for explanation of effects of irreversible interaction of laser radiation with semiconductors. For more detailed description, design and explanation of effects of irreversible interaction of laser radiation with semiconductors it is necessary to develop the methods of nonlinear dynamics [1].

Straight method of the estimation the energetic characteristics this processes may be realized in the next way. Energy of "disruption" of chemical bonds of one type is equalled [1]

$$E_{di} = N_i E_i, \tag{12}$$

where N_i – a density of proper bonds; E_i – energy of a disruption (ionization) one bond.

For the *InSb* $N_1 = N_2 = N_3 = {N_0}/{2}$ and are equalled $1.4 \cdot 10^{22} cm^{-3}, E_1 = E_g = 0.18 eV$ and therefore $E_{d1} = N_1 E_g = 403.2 \, {}^{J}/_{cm^3}$ and $E_{d2} = N_1 E_2 = 4368 \, {}^{J}/_{cm^3}$. Surface density of irradiation may be determined with the help of next formula

$$E_{sis} = \frac{E_{di}}{\alpha_i}, \tag{13}$$

where α_i – proper absorption factor, for the first bonds of *InSb* $\alpha_1 = 2 \cdot 10^5 cm^{-1}$, for second – $\alpha_2 = 10^5 cm^{-1}$. Second absorption factor is nonlinear and take into account the effect of blooming. For *InSb* these values are next $E_{s1s} = 0.002 \, {}^{J}/_{cm^2}$ and $E_{s2s} = 0.04368 \, {}^{J}/_{cm^2}$. These values must be multiplied on 2 (with including reflection) and therefore real values are next $E_{s1sr} = 0.004 \, {}^{J}/_{cm^2}$, $E_{s2sr} = 0.087974 \, {}^{J}/_{cm^2}$ and $E_{\Sigma r(2)} = 0.092 \, {}^{J}/_{cm^2}$. Energy of "disruption" of third chemical bonds (Fig. 2) is equaled $E_{d2} = N_1 E_3 = 4816 \, {}^{J}/_{cm^3}$. If $\alpha_3 = 10^5 cm^{-1}$ we have $E_{s3s} = 0.04816 \, {}^{J}/_{cm^2}$ and $E_{s3sr} = 0.096 \, {}^{J}/_{cm^2}$. Summary surface density of energy of three bonds is equaled $E_{\Sigma r(3)} = 0.188 \, {}^{J}/_{cm^2}$. Value $E_{\Sigma r(2)} = 0.092 \, {}^{J}/_{cm^2}$ is represented of curve 2 of Figure 1 and $E_{\Sigma r(3)} = 0.188 \, {}^{J}/_{cm^2}$ – curve 3 of Figure1 [1].

Now we are representing typical experimental data of Figure 4, which are received after laser irradiation of *Si* (duration of pulse 30 *ns*, wavelength 0.248 *nm*) [16, 17].

For explanation these results next model was created [1]. The question about the influence of saturation of excitation on effects of RO may be represented as process of transitions between stable and metastable phases too. Now we'll estimate the influence of parameters of irradiation (including spectral) on irreversible changes and transformations in *Si* and *Ge*.
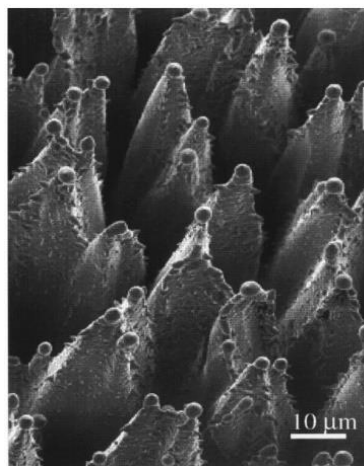

Figure 4. *Walled Si structure produced by 2040 laser pulses at E_d =1.5 J/cm² in 1 atm of SF₆ [16, 17].*

Now we'll be estimated intensities of Ruby and Neodymium laser irradiation (wavelengths of irradiation are 0,69 *μm* and 1,06 *μm* properly) of silicon and germanium, which are necessary for the creation of proper irreversible changes in irradiated semiconductor. As shown in [1], absorbance of the Neodimium laser radiation in silicon is equaled 60 *cm*⁻¹, Ruby – 2·10³ *cm*⁻¹.

Crystal semiconductors *Si* and *Ge* have, basically, the structure of diamond. Elementary lattice have 8 atoms. Volume density of elementary lattices may estimate according to formula [1]

$$N_L = \frac{\rho N_A}{8A}, \tag{14}$$

where ρ – density of semiconductor, N_A – Avogadro number, A – a weight of one gram-atom. For Si $N_{LSi} = 6.26 \cdot 10^{21} cm^{-3}$, and for Ge $N_{LGe} = 5.68 \cdot 10^{21} cm^{-3}$ [1].

The explanation of the experimental results for silicon and germanium was carried out using the phase diagram of Figure 5 [18].

However, Si and Ge may be crystallized in lattices with hexagonal, cubic and tetragonal symmetry. Phase diagram of Si as function of coordination number is represented on Figure 5 [18]. Coordination number (CN) 8 is corresponded of diamond lattice, CN 6 – hexagonal lattice, CN 4 – cubic lattice, CN 3 – trigonal lattice. It should be noted that melting temperatures of these phases are various.
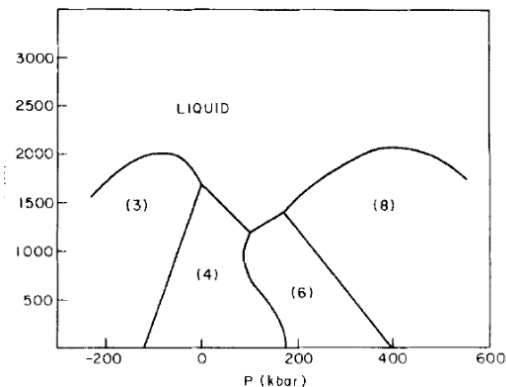

Figure 5. *A schematic phase diagram for Si(CN). The coordination numbers (CN) of the various phases are indicated. The diagram is based on common features of the phase diagrams of column IV elements as described by the references cited in Pistorius's review (Ref. 8 in [18]). Starting from a high tempera-ture $>3{\times}10^3 K$ and subject to a constraint of average density $\rho = \rho(4)$, a hot micronucleus will tend to bifurcate into the most stable phases (highest T_m) which straddle Si(4) in density. These are Si(3) and Si(8), as indicated by the diagram [18].*

Roughly speaking, transition from one phase to another for regime of saturation of excitation may be modeled as one-time breakage of proper number of chemical bonds, which are corresponded to the difference of CN of proper phases. For example, two bonds breakage is caused the phase transition from diamond to hexagonal structure. One bond breakage in the regime of saturation is caused to generation of laser radiation.

Results of calculation of volume densities of energy, which are necessary for breakage of proper number of bonds in regime of saturation of excitation, are represented in Table 1. It conceded that energies of all chemical bonds for elementary lattice are equivalent (*Si* and *Ge* are pure homeopolar semiconductors) [1]. For silicon energy of covalent bonds *Si-Si* are equaled 1,2–1,8 *eV*; for germanium energy of covalent bonds *Ge–Ge* are equaled 0,9–1,6 *eV*. Minimal values of these energies are corresponded of Pauling estimations.

Table1. *Volume density of energy I_{vi} (10^3 J/cm^3), which is necessary for the breakage of proper number of chemical bonds in the regime of saturation of excitation in Si and Ge [1]*

Materials	I_{v1}	I_{v2}	I_{v4}	I_{v5}
Si	1,18 – 1,76	2,36–3,54	4,72–7,08	5,90–8,84
Ge	0,80 - 1,42	1,60-2,84	3,20-5,68	4,00-7,12

Surface density of energy of Ruby and Neodimium lasers irradiation may receive after division of results of Table 2 on proper absorbance. Results of these calculations are represented in Table 2.

Table2. *Surface density of energy I_{si} (J/cm^2), which are necessary for the breakage of proper numbers of chemical bonds in Si and Ge crystals after Ruby and Nd lasers irradiation in regime of saturation the excitation [1]*

Conditions of irradiation	I_{s1}	I_{s2}	I_{s4}	I_{s5}
Si, Nd laser	19,67–30	39,34–60	78,68–120	98,35–150
Si, Ruby laser	0,59–0,89	1,18–1,76	2,36–3,54	2,95–4,42
Ge, Nd laser	0,050–0,089	0,100–0,178	0,200–0,356	0,250–0,445
Ge, Ruby laser	0,004–0,007	0,008–0,014	0,016–0,028	0,020–0,035

Remark to Table 2: absorbtances of *Si* (Neodimium laser) –60 cm^{-1}; *Si* (Ruby laser) – $2{\cdot}10^3$ cm^{-1}; *Ge* (Neodimium laser) – $1.6{\cdot}10^4$ cm^{-1}; *Ge* (Ruby laser) –$2{\cdot}10^5$ cm^{-1}.

These models were used to explain hedgehog-like structures of Figure 4. It should be noted that similar structures are also formed upon the irradiation 400 laser pulses with duration 130 fs and wavelength 0.8 μm [22]. However, the photon efficiency of excimer laser irradiation with nanosecond pulses is several times larger. Such models can also be using to obtain black silicon using laser technologies [13].

Using such physical-chemical models, the enrichment of laser-irradiated the near-surface layers of titanium with the hexagonal modification of this material was explained; while when titanium is heated to a temperature of 800 C, it completely transitions to the cubic modification [21]. As shown in [7] the cascade model of excitation of chemical bonds in the excitation saturation mode, it has been successfully used for plastics.

Now we estimate a role of physical-chemical processes in the generation of laser-induced optical breakdown in solid [8]

Two damages region in a crystal with moderately high density of inclusions were received in [26] for potassium chloride KCl after irradiation by CO_2-laser pulses (wavelength 10,6 μm, duration of pulse 30 ns). The laser was known to be operating in the lowest-order transverse Gaussian mode. There were several longitudinal modes, however, which contributed a time structure to the pulse, periodic at the cavity round-trip time. The phase relationships between the longitudinal modes varied from shot to shot, changing the details of the time structure and causing the peak of the envelope to fluctuate by ±15% [26]. These results are presented in Figure 6 [26].

Successive laser shot (1/sec) were focused into bulk single crystals using a 1-inch focal length "Irtran 2" lens [26]. The breakdown was monitored by observing the visible light from the focal region and by examining the damaged region under the microscope. It was found that most of the crystals suffered some damage even at relatively low power levels. The threshold of this type of damage varied by an order magnitude from one position in the crystal to another. At any particular energy level, damage would occur on the first laser shot or not at all. Figure 6 (a) shows that spatial inhomogeneities are in fact inclusions [26] . The damage bubbles occur randomly near, not necessarily in, the tiny focal volume. At a well-defined power threshold, an elongated pointed bubble forms, its vertex falling at the focus (Fig. 6 (b)). This power level is regarded as the bulk intrinsic breakdown threshold. Its value is reproducible in crystals from different manufacturers, with inclusions or without. When no inclusion free samples of a compound were available, the considerations mentioned above were using to determine the dielectric strength [26].
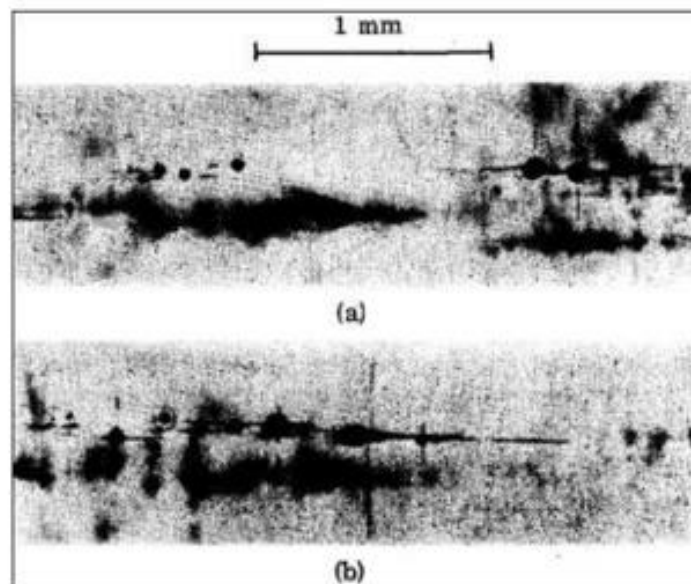

Figure6. *Two damages region in a crystal KCl with moderately high density of inclusions. The round black objects are bubbles. The radiation, incident from left to right, was yust at the intrinsic breakdown threshold. In one case (a) there was damage only at the inclusions. In (b), intrinsic breakdown occurred as evidenced by the pointed bubble. The straight lines represent cleavage [26].*

Experimental data, which are included microscopic structure of optical breakdown, are represented in Figure 7 and Figure 8 [15, 16].
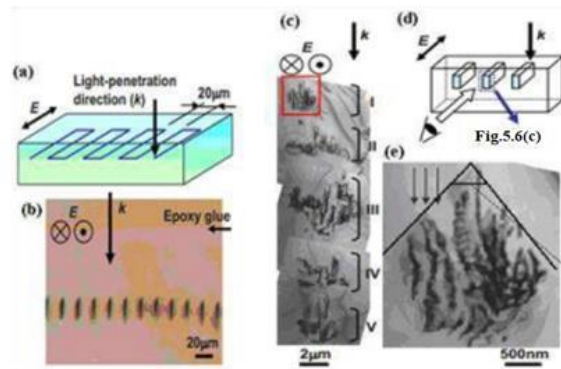
Figure7. (a) *Schematic illustration of the laser irradiated pattern. The light propagation direction (k) and electric field (E) are shown.* **(b)** *Optical micrograph of the mechanically thinned sample to show cross sections of laser-irradiated lines (200 nJ/pulse).* **(c)** *Bright-field TEM image of the cross section of a line written with pulse energy of 300 nJ/pulse.* **(d)** *Schematic illustration of a geometric relationship between the irradiated line and the cross-sectional micrograph.* **(e)** *Magnified image of a rectangular area in* **(c)** *[15, 16].*

Sectional area of receiving structures was ~ 22 μm, the depth of ~ 50 μm. As seen from Figure 7 (c) we have five stages disordered regions, which are located at a distance from 2 to 4 μm apart vertically [15, 16]. Branches themselves in this case have a thickness from 150 to 300 nm. In this case there are lines in the irradiated nanocavity with spherical diameter of from 10 nm to 20 nm. In this case, irradiated structures have crystallographic symmetry of the initial structure. In this case diffraction processes may be generated in two stages: 1- formation of diffraction rings of focused beams [8, 15, 16] and second-formation of diffracting gratings in the time of redistribution of second-order Cherenkov radiation [8, 15, 16] . Second case is analogous to the creation of self-diffraction gratings in NLO, but for Fig. 7 (c) and Fig. 8(b) our gratings are limited by much cone of Cherenkov radiation. Roughly speaking only Figure 7 (e) and Fig. 8 are represented "clean" breakdown.
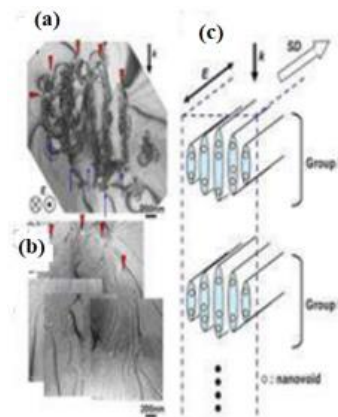

Figure8. *Laser-modified layers with a spacing of 150 nm are indicated by arrows. (a) Bright-field TEM image of a portion of the cross section of a line written with a pulse energy of 200 nJ/pulse. (b) Zero-loss image of a same area as in (a) with nanovoids appearing as bright areas. Correspondence with (a) is found by noting the arrowheads in both micrographs. (c) Schematic illustrations of the microstructure of a laser modified line. Light-propagation direction (k), electric field (E), and scan direction (SD) are shown. Only two groups (groups I and II) of the laser-modified microstructure are drawn [15, 16].*

The Cherenkov radiation may be certified with macroscopic and microscopic ways [8, 9].

First, macroscopic may be represented according to [19]. The similarity between charge particle and light-induced Cherenkov radiation one can invoke the analogy between Snell's law and Cherenkov radiation [19]. This natural since both effects can be derived in the same way from the Huygens interference principle. In [19] the point of intersection of a light pulse impinging at an angle φ on a boundary between two media moves with velocity $V = \frac{c}{n_1 \cos\varphi}$ This relation with Snell's law, gives the Cherenkov relation (Golub formula) [19].

$$\cos\theta = {c}/{n_2(\omega)V}.$$ (15)

This formula allows explain the angle differences for various type of Cherenkov radiation. In this case V may be represented as velocity of generation the optical-induced polarization too [8, 9, 13].

Thus, the refraction law a light at the boundary between two media is the same as the condition for Cherenkov emission by a source moving along the boundary. In nonlinear medium the emitted frequencies may be differ from the excitation frequency. The Cherenkov relation is still valid since the constructive interference occurs at a given Cherenkov angle for each Fourier frequency component of the light-induced nonlinear polarization. In a sense, one can speak about a nonlinear Snell-Cherenkov effect [19].

The microscopic mechanism of laser-induced Cherenkov radiation is expansion and application of Aage Bohrs microscopic theory of Cherenkov radiation [20] as part of deceleration radiation on optical case [8]. For optical case the Bohrs hyperboloid [20] must be changed on Gaussian distribution of light for mode TEM_{00} or distribution for focused light of laser beam [8, 9]. In this case, Cherenkov angle may be determined from next formula

$$\theta_{ch} + \alpha_{ir} = \pi/2 \text{ or } \theta_{ch} = \pi/2 - \alpha_{ir}, \tag{16}$$

where α_{ir} – angle between tangent line and direction of laser beam.

Angle α_{ir} was determined from next formula [8, 9]

$$\tan\alpha_{ir} = d_b/l_f, \tag{17}$$

where d_b – diameter of laser beam, (7 mm), l_f – length of focusing or self-focusing. In our case α_{ir} is angle of focusing or self-focusing.

This formula is approximate for average angle α_{ir}.

The Golub formula (13) was used for the determination product $n_2(\omega)V_{nlpol}$ [8, 9].

Thereby microscopic modified A. Bohr theory and macroscopic Golub model are mutually complementary methods [8, 9].

For the estimations of maximal radius of nanovoids we must use modified Rayleygh formula [8, 9]

$$R_{max} = \frac{2R}{0.915r} \sqrt{\frac{E_{ir}}{\pi\tau_{ir}cE}}, \tag{18}$$

where T_c – the time of creation the nanovoid (bubble), R is radius of nanovoid, r – radius of irradiated zone, E – Young module, E_{ir} – energy of one pulse. τ_{ir} – duration of irradiation pulse [8, 9].

If we substitute $r = 250$ nm, $R = 10$ nm, E=600 GPa [8], E_{ir}=300 nJ, $\tau_{ir} = 130$ ps, c =3·10^8 m/s, than have R_{max}=11 nm (Figure 8 (c)).

The speed of shock waves for femtosecond regime of irradiation is less as speed of sound. However, we have two speeds of sound in elastic body: longitudinal v_{ls} and transversal v_{ts} [8, 9]. Its values are determined with next formulas

$$v_{ls} = \sqrt{\frac{E(1-v)}{\rho_0(1+v)(1-2v)}}, \text{ and } v_{ts} = \sqrt{\frac{E}{\rho_0(1+v)}}, \tag{19}$$

where v – Poisson's ratio [8, 9]. The ratio between of these two speeds is equaled

$$\alpha = \frac{v_{ts}}{v_{ls}} = \sqrt{\frac{(1-2v)}{2(1-v)}}. \tag{20}$$

However, this ratio must be true for shock waves too. Therefore, for silicon carbide for $v = 0,45$ [8, 9] and $\alpha = 0,33$. Roughly speaking last ratio is determined the step of ellipsoidal forms of our nanovoids (Figure 8 (c)).

In [8, 9] allow estimating maximal longitudinal and transversal $R_{maxi}, i \in (l, t)$. These values are 6 nm and 19 nm properly.

In this case we represented 4H-SiC as isotropic plastic body. For real picture we must represent hexagonal structure. But for the qualitative explanation of experimental data of Fig. 8 this modified Rayleygh model allow explaining and estimating the sizes and forms of receiving nanovoids [8, 9].

Laser-induced shock processes have specific peculiarities. In general case we have electromagnetic and acoustic shock processes [8]. Formally, these processes have similar nature. Speed of electromagnetic shock processes (speed of polarization the media in the result of corresponding interaction) must be more as phase speed of light in media. In this case phase speed of light in media has next physical nature: it is speeding of collectivization the electromagnetic oscillations for proper frequency. Roughly speaking it is electromagnetic characteristic of media, which is corresponded to its electron and ion subsystems. Example of this type process is Cherenkov radiation. In this case, we have radiated reaction of media on heterogeneity excitation of media in shock regimes of interactions. Speed of acoustic shock processes (speed of motion proper object in media) must more as speed of sound in media [8]. Nevertheless, speed of sound is media is average heat speed of media, which is connected with atomic structure of media. Examples of these processes are: flight of airplane or rocket in with supersonic speed; various explosions. Roughly speaking, explosions may be characterized as chemical process with speed more as sound speed in media. Mach number is characterized in this case the macroscopic "detonation" of corresponding process. Both processes (electromagnetic and acoustic) are characterized by Much cone, which is created by proper vectors of speed processes or object and speed characteristic of media (polarization or sound) [8]. Laser-induced shock processes may be represented as analogous to acoustic explosions. However, this process is realized with electromagnetic speed. In this case, we must have "electromagnetic" explosion as Cherenkov radiation [8]. Due to the similarity of electromagnetic and acoustic processes of kinetic processes, we can use both to estimate the parameters of impact processes, to determine the size of nanovoids, using the electromagnetic modified Rayleigh model (formula (18)) and to determine the shape of nanovoids, acoustic formula (18 a).

$$R_{max}^{ac} = \frac{2R}{0.915r}\sqrt{\frac{E_{ir}}{\pi\tau_{ir}c_s E}}, \qquad\qquad (18\ a)$$

where c_s is speed of sound.

Speed of electromagnetic shock processes (speed of polarization the media in the result of corresponding interaction) must be more as phase speed of light in media. In this case phase speed of light in media has next physical nature: it is speeding of collectivization the electromagnetic oscillations for proper frequency. Roughly speaking it is electromagnetic characteristic of media, which is corresponded to its electron and ion subsystems. Example of this type process is Cherenkov radiation. In this case, we have radiated reaction of media on heterogeneity excitation of media in shock regimes of interactions [8, 9].

Speed of acoustic shock processes (speed of motion proper object in media) must more as speed of sound in media [8]. However, speed of sound is media is average heat speed of media, which is connected with atomic structure of media. Examples of these processes are next: flight of airplane or rocket in with supersonic speed; various explosions. Roughly speaking, explosions may be characterized as chemical process with speed more as sound speed in media. Mach number is characterized in this case the macroscopic "detonation" of corresponding process.

Both processes (electromagnetic and acoustic) are characterized by Much cone, which is created by proper vectors of speed processes or object and speed characteristic of media (polarization or sound) [8].

Laser-induced shock processes may be represented as analogous to acoustic explosions. However, this process is realized with electromagnetic speed. In this case, we must have "electromagnetic" explosion as Cherenkov radiation [8].

We used next approximations. Photography of Figure 6 gives a blurry image compared to the bright-field TEM image of Figure 7. Therefore, we can't see the microstructure of optical breakdown for Figure 6. In addition, we use rough average approximations for diameter $d_{average}$ and length l of cascade laser-induced optical breakdown of Figure 6 [8, 26]. Volume of cascade was determined as cylinder volume.

Figure 6 is similar to Figure 7 (c). However, regimes of irradiation of Figure 6 are similar to mode TEM_{01} [26]. Therefore, we have two channels of generation the cascade of laser-induced optical breakdown [8].

The distances between bubbles of Figure 6 (b) are more as between regions of destruction of Figure 7 (c). Nevertheless, conditions of focusing the radiation in these both cases are equivalence. Therefore, the

distances between neighboring bubbles l_2 of Figure 6(b) and neighboring regions of destruction l_1 of Figure 7(c) are connecting by next formula [8]

$$l_2 = \frac{\lambda_2 \tan\left(\varphi_1/2\right)}{\lambda_1 \tan\left(\varphi_2/2\right)} l_1. \tag{21}$$

In whole, the correlation of these distances is depended from wavelength of irradiation and focusing angles, including intensity of irradiation. Which is determined the step of homogeneity of irradiated matter. If we substitute in formula (21) $\lambda_2 = 10.6\ \mu m$ and $\lambda_1 = 0.8\ \mu m$ and $\varphi_1 = \varphi_2$ then we'll receive

$$l_2 = 13.25 l_1. \tag{21a}$$

Energy characteristics of irradiation of potassium chloride had value 2 *J/pulse* from [8, 26]. In this case, we have effective using energy. Methods of estimations of energy characteristics for *KCl* are rougher as for 4H-*SiC* [8]. However, we must suppose that focused laser irradiation has diffraction stratification, generation of Cherenkov radiation and interference of this Cherenkov radiation. On Figure 6 (b) we see 5-7 steps of cascade optical breakdown. Sources of Cherenkov radiation are diffraction stratified cones [8].

If this scenario is true, we have as for 4H-SiC effective transformation the energy of laser radiation to cascade of laser-induced breakdown for *KCl* too. This value is 11,6 – 17,4 percents [8].

We can estimate sizes and forms of possible nanovoids for potassium chloride too. Let us take the ratio of the radius of the irradiation zone to the radius of the nanowire as 50. The energy of irradiation is 2 *J* [26]. The duration of irradiation is 30 *ns* [26]. For *KCl* Young's modulus is equaled 29.67 *GPa*, Poisson's ratio – 0.216 [8].

After substitution of these data to formula (18) we have $R_{maxKCl} = 62.5 nm$. The ellipticity of *KCl* nanovoids may be determined from (20) $\alpha_{KCl} = 0.6$ [8].

Let us now estimate the maximum bubble radii for the acoustic case. For this, in formula (18), you need to change the speed of light to the speed of sound (18 a).

As a result, we get $R_{maxSiC}^{ac} = 1.7 \mu m$ and $R_{maxKCl}^{ac} = 28 \mu m$. The shape of the voids does not change, they just increase in size by 2-3 orders of magnitude [8].

If we take the ratio of the acoustic formula (18 a) and the optical formula (18), then for the same irradiation modes we have the ratio

$$\frac{R_{max}^{ac}}{R_{max}} = \sqrt{\frac{c}{c_s}}. \tag{22}$$

However, a comparison with the experimental results (Figure 7) shows that the main role in the formation of nanovoids has electromagnetic processes [8]. This fact allows explaining by the fact that in this case a chain of close-range coherent processes of transformation of both optical radiation into the excitation of the medium and the corresponding relaxation of the medium is implemented, in other words, there is a chain of interconnected coherent transformations. Therefore, for this case it is appropriate to introduce the concepts of coherent zone and integral photon efficiency [8, 9].

In the acoustic case, the entire environment reacts, while the results of the interaction of light with matter managed to "collectivize" and that is why the result of the interaction can be considered as the result of the action of a quasi-classical body (in this case, a laser pulse) on the environment.

For modeling processes as laser-induced optical breakdown of a transparent material, we must also use physical-chemical modeling methods to establish the self-focusing mode and the actual optical breakdown at the maximum of the interferograms formed by the short-wavelength part of the secondary Cherenkov radiation. For the case of focused radiation irradiation, the first part of the modeling is not needed. In general, physical-chemical modeling methods more fully reflect the specifics of the interaction of laser radiation with matter at the microscopic level, including both the phenomena and processes of Nonlinear and Relaxed Optics. However, the main problem for this case is the question of converting optical radiation into conditions that actually lead to optical breakdown of the medium.

3. CONCLUSIONS

1. Necessary of introduction physical–chemical methods of modelling in Nonlinear and Relaxed Optical is analyzing.

2. Haken-Landau synergetic-thermodynamically, method in NLO is observing.

3. Adaptive photo-induced model and cascade model of excitation step-on-step corresponding chemical bonds in the regime of saturation the excitation were using for the explanation of macroscopic and microscopic nature of the creation subsurface laser-induced donor centers in *InSb* and *InAs*.

4. Cascade model of excitation step-on-step corresponding chemical bonds in the regime of saturation the excitation were using for the explanation the cascade phase transformation in *Si* and *Ge*.

5. The use of this models has been demonstrated for other materials, including metals and plastics/

6. Role of physical-chemical methods in the modeling laser-induced optical breakdown of matter are analyzing.

7. The questions about nature of electromagnetic shock processes of RO are observing.

REFERENCES

[1] Trokhimchuck P. P. (2016) Relaxed Optics: Realities and Perspectives. Lambert Academic Publishing, Saarbrukken

[2] Haken H. (1983) Synergetics. An itroduction, 3rd ed. Springer Verlag, Berlin, Heidelberg, New York, Tokio

[3] Perina J. (1991) Quantum statistics of linear and nonlinear optical phenomena, 2nd ed. Kluver Publishing; Dordrecht

[4] Andreev A. V., Emelyanov V. I., and Il'ynskiy Yu.A. (1988) Cooperative phenomena in optics. Nauka, . Moscow (In Russian)

[5] Wayne R. P. (1988) Principles and Applications of Photochemistry. University Press. Oxford

[6] Shen Y. R. (1984) The principles of Nonlinear Optics. Wiley-Interscience, New York

[7] Trokhimchuck P. P. (2020) Relaxed Optics: Modelling and Discussions. Lambert Academic Press, Saarbrukken

[8] Trokhimchuck P. P. (2024) Relaxed Optics: Modelling and Discussions 3. Bright Sky Publishers, New Dehli

[9] Trokhimchuck P. P. (2022) Relaxed Optics: Modelling and Discussions 2. Lambert Academic Press, Saarbrukken

[10] Trokhimchuck P. P. (2020) Role Physical-Chemical Processes in the Generation of Laser-Induced Structures. In: Research Trends in Chemistry. Ed. Ashok Kumar Acharya, vol. 11, ch.6., New Delhi: AkiNik Publications, 109 – 140.

[11] Trokhimchuck P. P. (2024) Some problems of modelling the physical-chemical processes in Relaxed Optics. AIP Conference Proceedings, vol. 3084(1), 080001, https://doi.org/10.1063/5.0200356.

[12] Laidier K. J. (1993) The World of Physical Chemistry. University Press, Oxford.

[13] Trokhimchuck P. P. (2024) Main Problems of Creation Laser-Induced Thin Films. In: Advances in engineering technology. Ed. Singh J., New Dehli, AjkiNik Publications, vol 8, ch.2, 15-46.

[14] Okada T., Tomita T., Matsuo S., Hashimoto S., Kashino R., Ito T. (2012) Formation of nanovoids in femtosecond laser irradiated single crystal silicon carbide. Material Science Forum , vol. 725, 19 – 22. https://doi.org//10.4028/www.scientific.net/MSF.725.19.

[15] Okada T., Tomita T., Matsuo S., Hashimoto S., Ishida Y., Kiyama S., Takahashi T. (2009) Formation of periodic strain layers associated with nanovoids inside a silicon carbide single crystal induced by femtosecond laser irradiation. J. Appl. Phys., v. 106, p.054307, 5 p. https://doi.org/10.1063/1.3211311.

[16] Pedraza A. J., Fowlkes J. D. and Lowndes D. H. (1999) Silicon microcolumn arrays growth by nanosecond pulse laser irradiation. Appl. Phys. Lett. 74(10), 2222-2224. https://doi.org/10.1063/1.123838.

[17] Pedraza A. J., Guan Y. F., Fowlkes J. D., and Smith D. A. (2004) Nanostructures produced by ultraviolet laser irradiation of silicon. I. Rippled structures. *J*. Vac. Sc. @ Techn. B., vol. 22, no. 6, 2823-2835, https://doi.org/10.1116/1.1821575; Guan Y. F., Pedraza A. J., Fowlkes J. D., and Joy D. A. (2004) II Nanoprotrusions and nanoparticles. J. Vac. Sci. Technol. B, vol. 22, no. 6, 2836–2843, https://doi.org/10.1116/1.1821576.

[18] Philips J. C. (1981) Metastable honeycomb model of laser annealing. Journal of Applied Physics, vol. 32, no. 12, 7397–7402. https://doi.org/10.1063/1.328729.

[19] Golub I. (1990) Optical characteristics of supercontinuum generation. Optics Letters, vol.15, no. 6, 305-307. https://doi.org/10.1364/OL.15.000305.

[20] Bohr A. (1948) Atomic interactions in penetration phenomena. Det. KGL Danske Videnskabernes Selskab. Matematisk-Fysiske Meddelelser, vol. XXIV (19), 1-52.

[21] Tsukamoto M., Asuka K, Nakano N., Hashida M., Ratto M., Abe N., and Fujita M. (2006) Period microstructures produced by femtosecond laser irradiation on titanium plate. Vacuum, 80, 1346-1350.

[22] Shen M., Carey J. E., Crouch C. H., Kandyla M., Stone H. A., and Mazur E.. (2008) High-density regular arrays of nano-scale rods formed on silicon surfaces via femtosecond laser irradiation in water. Nanoletters, vol. 8, no. 7, 2087-2091.

[23] Makin V. S. (2013) Peculiarities of the formation the ordered micro and nanostructures in condensed matter after laser excitation of surface polaritons modes. D. Sc. Thesis, State university of information technologies, mechanics and optics, Saint-Petersburg (In Russian)

[24] de Broglie L. (1964) Thermodynamics of isolated point (Hidden thermodynamics of particles). Gautrhier Villars, Paris

[25] Bogatyryov V. A., and Kachurin G. A. (1977) The creation low resistively n-layers on *InSb* with help the pulse laser irradiation. Physics and technical of semiconductors, vol.11, no. 7, 100-102. (In Russian)

[26] Yablonovich E.. (1971) Optical Dielectric Srength of AlkaliHalide Crystalls Obtained by Laserinduced Breakdown. Appl. Phys. Lett., vol. 19, no. 11, 495-497, 1971. https://doi.org/10.1063/1.1653788